

Numerical simulation of vortex dynamics in Ginzburg-Landau-Schrödinger equation

YANZHI ZHANG¹, WEIZHU BAO² and QIANG DU³

¹*Department of Mathematics, National University of Singapore, Singapore 117543
email: zhyanzhi@gmail.com*

²*Department of Mathematics and Center for Computational Science and Engineering
National University of Singapore, Singapore 117543*

email: bao@math.nus.edu.sg, URL: http://www.math.nus.edu.sg/~bao/

³*Department of Mathematics, Pennsylvania State University, University Park, PA 16802, USA
email: qdu@math.psu.edu, URL: http://www.math.psu.edu/qdu*

(Received 8 May 2007; revised 23 July 2007; first published online 4 September 2007)

The rich dynamics of quantized vortices governed by the Ginzburg-Landau-Schrödinger equation (GLSE) is an interesting problem studied in many application fields. Although recent mathematical analysis and numerical simulations have led to a much better understanding of such dynamics, many important questions remain open. In this article, we consider numerical simulations of the GLSE in two dimensions with non-zero far-field conditions. Using two-dimensional polar coordinates, transversely highly oscillating far-field conditions can be efficiently resolved in the phase space, thus giving rise to an unconditionally stable, efficient and accurate time-splitting method for the problem under consideration. This method is also time reversible for the case of the non-linear Schrödinger equation. By applying this numerical method to the GLSE, we obtain some conclusive experimental findings on issues such as the stability of quantized vortex, interaction of two vortices, dynamics of the quantized vortex lattice and the motion of vortex with an inhomogeneous external potential. Discussions on these simulation results and the recent theoretical studies are made to provide further understanding of the vortex stability and vortex dynamics described by the GLSE.

1 Introduction

The Ginzburg-Landau-Schrödinger equation (GLSE) is one of the most studied non-linear equations in the physics community. It describes a vast variety of phenomena from non-linear waves to second-order phase transitions, from superconductivity, superfluidity and Bose-Einstein condensation (BEC) to liquid crystals and strings in the field theory. A specific form of the GLSE we study here is given by:

$$(\alpha - i\beta)\partial_t\psi(\mathbf{x}, t) = \Delta\psi + \frac{1}{\varepsilon^2}(V_0(\mathbf{x}) - |\psi|^2)\psi, \quad \mathbf{x} \in \mathbb{R}^2, t > 0, \quad (1.1)$$

$$\psi(\mathbf{x}, 0) = \psi_0(\mathbf{x}), \quad \mathbf{x} \in \mathbb{R}^2, \quad (1.2)$$

with nonzero far-field conditions

$$|\psi(\mathbf{x}, t)| \rightarrow 1 \text{ (e.g. } \psi \rightarrow e^{im\theta}), \quad t \geq 0, \quad \text{when } r = |\mathbf{x}| = \sqrt{x^2 + y^2} \rightarrow \infty; \quad (1.3)$$

here t is time, $m \in \mathbb{Z}$ is a given integer, $\mathbf{x} = (x, y) \in \mathbb{R}^2$ is the Cartesian coordinate vector, (r, θ) is the polar coordinate system, $\psi(\mathbf{x}, t)$ is a complex-valued wave function, $V_0(\mathbf{x})$ is a given real-valued external potential satisfying $V_0(\mathbf{x}) \rightarrow 1$ when $|\mathbf{x}| \rightarrow \infty$, ε is a positive constant and α and β are two nonnegative constants satisfying $\alpha + \beta > 0$.

The equation (1.1) covers many non-linear equations arising in various different applications. For example, when $\alpha=1$ and $\beta=0$, it collapses to the non-linear heat equation (NLHE) [36, 37] or the Ginzburg-Landau equation (GLE). The case of GLE with a complex order parameter is well known [1, 19, 20, 32] for modelling superconductivity, while the real-order parameter case corresponds to the so-called Allen-Cahn equation often used in phase transition studies [21]; when $\alpha=0$ and $\beta=1$, it reduces to the non-linear Schrödinger equation (NLSE) [35, 36, 40] for modelling, for example, superfluidity or BEC; when $\alpha > 0$ and $\beta > 0$, it is the complex Ginzburg-Landau equation (CGLE) or the NLSE with a damping term [5], which also arises in the study of the hydrodynamic instability [2]. When $V_0(\mathbf{x}) \equiv 1$, the external potential is uniform; when $V_0(\mathbf{x}) \not\equiv 1$, the medium is inhomogeneous [6, 25, 26, 34]. When $\varepsilon=1$, it is the standard GLSE, while for $0 < \varepsilon \ll 1$, it is the GLSE in the semi-classical regime.

The boundary condition (1.3) allows one to introduce the notation $\deg \psi$, that is, degree of ψ , as an index (winding number) at ∞ of ψ , considered as a vector field on \mathbb{R}^2 , that is,

$$\deg \psi = \frac{1}{2\pi} \int_{|\mathbf{x}|=R} d(\arg \psi), \quad (1.4)$$

for R sufficiently large. Based on this, an important quantity related to (1.1) is the rescaled free energy or Lyapunov functional equation.

$$E(\psi) = \int_{\mathbb{R}^2} \left[|\nabla \psi|^2 - \frac{(\deg \psi)^2}{r^2} \chi(r) + \frac{1}{2\varepsilon^2} (V_0(\mathbf{x}) - |\psi|^2)^2 \right] d\mathbf{x}, \quad (1.5)$$

where $\chi(r)$ is a smooth positive function on $[0, \infty)$ vanishing at $r=0$ and converging to one as $r \rightarrow \infty$. Thus, (1.1) can be written as

$$(\alpha - i\beta) \partial_t \psi(\mathbf{x}, t) = - \frac{\delta E(\psi)}{\delta \psi^*}, \quad (1.6)$$

where f^* denotes the conjugate of a function f . Thus, when $\alpha > 0$, the GLSE (1.1) is a dissipative system and the free energy decreases as time t increases, that is, $dE(\psi)/dt \leq 0$. On the other hand, when $\alpha=0$, it is a dispersive system and thus it is time-reversible and time-transverse invariant. Furthermore, the system admits at least two important invariants, which are the rescaled free energy

$$E(\psi(\cdot, t)) \equiv E(\psi(\cdot, 0)) = E(\psi_0), \quad t \geq 0 \quad (1.7)$$

and the rescaled density, respectively,

$$N(\psi(\cdot, t)) = \int_{\mathbb{R}^2} [|\psi(\mathbf{x}, t)|^2 - |\psi_0(\mathbf{x})|^2] d\mathbf{x} \equiv 0, \quad t \geq 0. \quad (1.8)$$

There have been many analytical and numerical studies recently that deal with vortex dynamics in the GLSE (1.1). For vortex dynamics in the GLE, that is, $\beta = 0$ in (1.1), Neu [36, 37] found numerically that vortices with winding number $m = \pm 1$ are dynamically stable and $|m| > 1$ dynamically unstable, respectively. Using asymptotic analysis, he showed that a pair of vortices evolving under the GLE with like (opposite) winding numbers undergoes a repulsive (attractive) interaction. Neu's studies were later extended by others [43, 44]. E [22] studied the dynamics of vortices in the GLE in the asymptotic limit when the vortex core size is much smaller than the inter-vortex distance, and derived reduced systems of ordinary differential equations (ODEs) governing the evolution of these vortices. Similar studies have also been done by Chapman and Richardson [11] and Weinstein and Xin [48] for the Ginzburg-Landau models of superconductivity. Lin [32, 33] rigorously proved vortex dynamic laws and showed that the energies of solutions in the GLE flow are concentrated at vortices in two-dimensions and filaments in three-dimension. Similar studies were conducted by Jerrard and Sonner [24]. Ovchinnikov and Sigal [38, 40–42] studied the energy of Ginzburg-Landau vortices and their asymptotic behaviour and examined the stability properties. The pinning effect of the vortices due to impurities was also established [25–27, 34]. For numerical solutions of the GLE and the related Ginzburg-Landau models of superconductivity, finite element methods (FEMs) were studied [13, 17, 19, 28]. Numerical results of interaction between a few vortices [18, 31, 34] and vortex lattices [16] as well as the stochastic dynamics [15] have been reported.

For vortex dynamics in the NLSE, that is, $\alpha = 0$ in (1.1), Neu [36] found that the vortices behave like point vortices in ideal fluid and obtained the Hamiltonian equations for governing dynamics of the vortex centres. Lin and Xin [35] derived a vortex motion law in the incompressible fluid limit on a bounded domain with Dirichlet or Neumann boundary condition. Colliander and Jerrard [14] investigated vortex structures in a torus. Ovchinnikov and Sigal [39, 40] studied vortex structure of the corresponding solutions as well as corrections due to radiation, and derived equations for the vortex dynamics and radiation by using the methods of effective action and geometric solvability. Furthermore, they analytically obtained the dynamical patterns of two vortices with like (opposite) winding numbers in the NLSE when the initial distance between them is large enough by solving the governing Hamiltonian equations [39]. Because of the dispersive nature of the NLSE and highly oscillating nature in transverse direction of the nonzero far-field boundary condition (1.3), it is extremely difficult to solve (1.1)–(1.3) numerically. To our knowledge, there is no conclusive numerical result reported in the literature for vortex stability and interaction in the NLSE. In fact, the dynamical stability of vortices as solutions of the NLSE remains largely an open problem [36].

To study effectively the stability and dynamics of vortices as solutions of the GLSE (1.1), especially for dynamics of vortex lattices, accurate and reliable numerical simulations can be an important tool. Currently, the numerical methods proposed in the literature for studying vortex dynamics in the GLSE remain limited [13, 17, 36], with most of them being low-order methods. Thus, it is of much interest to develop an efficient, accurate and unconditionally stable numerical method for the GLSE (1.1) with nonzero far-field conditions (1.3). We propose such a numerical method here and apply it to study vortex dynamics in the GLSE. The key features of our numerical method include (i) the application of a time-splitting technique for decoupling the nonlinearity in the GLSE;

(ii) the adoption of polar coordinates so as to effectively match and resolve the non-zero far-field conditions (1.3) in phase space; and (iii) the utilization of Fourier pseudo-spectral discretization in the transverse direction and a second- or fourth-order finite difference or finite element discretization in the radial direction. The proposed numerical method is similar to the one used to study the dynamics of rotating BEC [3, 4], where the angular momentum rotation term becomes a constant with the adoption of polar coordinates. The extensive numerical results presented in this article demonstrate that the method is very efficient and accurate, and when applied to study interaction and dynamics of vortex lattices in the GLSE (1.1), it is capable of producing conclusive simulation results on the vortex stability and dynamic properties. These simulation results not only give substantiation to some existing analytical studies while revealing their range of validity but also provide new insight into the details of the stability and dynamic behaviour beyond those currently known in the literature.

The article is organized as follows. In Section 2, we briefly review the vortex states of the GLSE and their numerical computation. In Section 3, a new numerical method is presented for the efficient and accurate simulation of the GLSE (1.1)–(1.3) in two-dimensions. It is then applied to study dynamics of vortex states, the interaction of two vortices with winding number $m = \pm 1$ and the dynamics of vortex lattices in the GLSE in Section 4. Finally, some conclusions are drawn in Section 5.

2 Stationary vortex states

For the convenience of the reader, here we review the stationary vortex states of GLSE (1.1) studied in [12, 36], that is, we consider the GLSE (1.1) in the time-independent case with $\varepsilon = 1$ and $V_0(\mathbf{x}) \equiv 1$:

$$\Delta\phi(\mathbf{x}) + (1 - |\phi(\mathbf{x})|^2)\phi(\mathbf{x}) = 0, \quad \mathbf{x} \in \mathbb{R}^2, \quad (2.1)$$

$$|\phi(\mathbf{x})| \rightarrow 1, \quad \text{when } |\mathbf{x}| \rightarrow \infty, \quad (2.2)$$

where $\phi(\mathbf{x})$ is a complex-valued function and can be viewed as the steady-state solution of the GLSE (1.1). It is known that there are *vortex solutions* with a single winding number or index $m \in \mathbb{Z}$, which take the form

$$\phi_m(\mathbf{x}) = f_m(r) e^{im\theta}, \quad \mathbf{x} = (r \cos(\theta), r \sin(\theta)) \in \mathbb{R}^2. \quad (2.3)$$

The modulus $f_m(r)$ satisfies the boundary value problem

$$\frac{1}{r} \frac{d}{dr} \left(r \frac{df_m(r)}{dr} \right) - \frac{m^2}{r^2} f_m(r) + (1 - f_m^2(r)) f_m(r) = 0, \quad 0 < r < \infty, \quad (2.4)$$

$$f_m(0) = 0, \quad f_m(r) = 1, \quad r \rightarrow \infty. \quad (2.5)$$

The asymptotic behaviour of $f_m(r)$ as $r \rightarrow 0$ and $r \rightarrow \infty$ can be respectively estimated as follows [36]:

$$f_m(r) \sim \begin{cases} a r^{|m|} + O(r^{|m|+2}), & \text{as } r \rightarrow 0, \\ 1 - \frac{m^2}{2r^2} + O\left(\frac{1}{r^4}\right), & \text{as } r \rightarrow \infty, \end{cases} \quad (2.6)$$

where a is a constant.

Table 1. Core size of the vortex states for different winding number m

| Winding number | $m = \pm 1$ | $m = \pm 2$ | $m = \pm 3$ | $m = \pm 4$ |
|-------------------|-------------|-------------|-------------|-------------|
| Core size r_m^0 | 1.75 | 3.3674 | 4.9128 | 6.4303 |

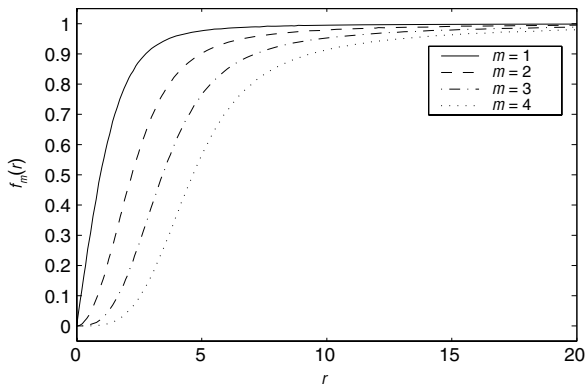


FIGURE 1. Numerical solution of modulus $f_m(r)$ for different winding numbers m .

To find these vortex states numerically, we first truncate the problem (2.4)–(2.5) into a bounded interval $r \in [0, R]$, with sufficiently large R and set an artificial boundary condition $f_m(R) = 1$ at $r = R$. Then we discretize the equation (2.4) by the second-order finite difference method and solve the non-linear system by Newton iteration. We note that a shooting method can also be employed to obtain such solutions [12, 29]. Figure 1 shows the numerical results of $f_m(r)$ for different winding numbers m . On the basis of our numerical results in Section 4, we hereby define the core size r_m^0 of a vortex state with winding number m by the condition $f_m(r_m^0) = 0.755$. Table 1 lists the core sizes of vortex states with different winding number m , in particular, we have $r_1^0 \approx 1.75$.

For the equation (2.1)–(2.2) with a specified degree condition, solutions of the form (2.3) are the only vortex solutions known in the literature, the question whether there are other symmetry breaking solutions in the whole space remains open. A recent exploration of this issue was done by Ovchinnikov and Sigal [42].

3 Numerical methods

In this section, we present an efficient, accurate and unconditionally stable numerical method for solving the GLSE (1.1)–(1.3). In the practical implementation, we truncate the problem (1.1)–(1.3) to one defined in a bounded computational domain with an inhomogeneous Dirichlet boundary condition:

$$(\alpha - i\beta)\partial_t \psi(\mathbf{x}, t) = \Delta \psi + \frac{1}{\varepsilon^2} [V(\mathbf{x}, t) - |\psi|^2] \psi, \quad \mathbf{x} \in \Omega_R, \quad t > 0, \quad (3.1)$$

$$\psi(\mathbf{x}, t) = e^{im\theta}, \quad \mathbf{x} \in \Gamma = \partial\Omega_R, \quad t \geq 0, \quad (3.2)$$

$$\psi(\mathbf{x}, 0) = \psi_0(\mathbf{x}), \quad \mathbf{x} \in \bar{\Omega}_R; \quad (3.3)$$

where we choose $\Omega_R = \{(x, y), r = \sqrt{x^2 + y^2} < R\}$ with sufficiently large R and $V(\mathbf{x}, t) = V_0(\mathbf{x}) + W(\mathbf{x}, t)$ with $W(\mathbf{x}, t)$ as an external driven potential. In our simulations, a sufficiently large R is chosen to ensure that the effect of domain truncation remains insignificant. The use of more sophisticated radiation boundary conditions is an interesting topic that remains to be examined in the future.

3.1 Time splitting

Historically, time-splitting methods are among most popular methods for studying the dynamics of GLSE, in particular, NLSE (see earlier studies [10, 46, 47] and the references therein as well as recent developments and applications [5, 7–9]). For more general discussions on splitting methods, we refer to references [23, 45]. Let $\Delta t > 0$ be the step size for time discretization. For $n = 0, 1, 2, \dots$, from time $t_n = n\Delta t$ to $t_{n+1} = t_n + \Delta t$, the GLSE (3.1) is solved in two splitting steps. One first solves

$$(\alpha - i\beta)\partial_t \psi(\mathbf{x}, t) = \Delta \psi, \tag{3.4}$$

for the time step of length Δt , followed by solving

$$(\alpha - i\beta)\partial_t \psi(\mathbf{x}, t) = \frac{1}{\varepsilon^2}(V(\mathbf{x}, t) - |\psi|^2)\psi, \tag{3.5}$$

for the same time step. Equation (3.4) is discretized in the next subsection. For $t \in [t_n, t_{n+1}]$, we easily obtain the following ODE for $\rho(\mathbf{x}, t) = |\psi(\mathbf{x}, t)|^2$:

$$\partial_t \rho(\mathbf{x}, t) = \eta[V(\mathbf{x}, t)\rho(\mathbf{x}, t) - \rho^2(\mathbf{x}, t)], \quad \mathbf{x} \in \Omega_R, \quad t_n \leq t \leq t_{n+1}, \tag{3.6}$$

where $\eta = 2\alpha/\varepsilon^2(\alpha^2 + \beta^2)$. Denote $V_n(\mathbf{x}, t) = \int_{t_n}^t V(\mathbf{x}, \tau) d\tau$, we can solve (3.6) to get

$$\rho(\mathbf{x}, t) = \frac{\rho(\mathbf{x}, t_n) \exp[\eta V_n(\mathbf{x}, t)]}{1 + \eta \rho(\mathbf{x}, t_n) \int_{t_n}^t \exp[\eta V_n(\mathbf{x}, \tau)] d\tau}. \tag{3.7}$$

Consequently, in the special case $V(\mathbf{x}, t) = V_0(\mathbf{x})$, i.e. $W(\mathbf{x}, t) \equiv 0$, we have some exact analytical solutions given by

$$\rho(\mathbf{x}, t) = \begin{cases} \rho(\mathbf{x}, t_n), & \alpha = 0, \\ \frac{\rho(\mathbf{x}, t_n)}{1 + \eta \rho(\mathbf{x}, t_n)(t - t_n)}, & V_0(\mathbf{x}) = 0 \ \& \ \alpha \neq 0, \\ \frac{V_0(\mathbf{x})\rho(\mathbf{x}, t_n)}{\rho(\mathbf{x}, t_n) + (V_0(\mathbf{x}) - \rho(\mathbf{x}, t_n)) \exp[-\eta V_0(\mathbf{x})(t - t_n)]}, & V_0(\mathbf{x}), \alpha \neq 0. \end{cases} \tag{3.8}$$

For the phase angle $S(\mathbf{x}, t)$ (determined as $\psi = \sqrt{\rho}e^{iS}$), we have the equation

$$\partial_t S(\mathbf{x}, t) = \frac{\beta}{\varepsilon^2(\alpha^2 + \beta^2)} [V(\mathbf{x}, t) - \rho], \quad \mathbf{x} \in \Omega_R, \quad t_n \leq t \leq t_{n+1}. \tag{3.9}$$

For $\alpha \neq 0$, by (3.6), the above equation is equivalent to

$$\partial_t S = \frac{\beta}{2\alpha} \partial_t \ln \rho, \quad \mathbf{x} \in \Omega_R, \quad t_n \leq t \leq t_{n+1}. \quad (3.10)$$

Plugging (3.7) into (3.5), we get for $t \in [t_n, t_{n+1}]$,

$$\psi(\mathbf{x}, t) = \psi_n(\mathbf{x}, t_n) \sqrt{U_n(\mathbf{x}, t)} \exp \left[\frac{i\beta}{\varepsilon^2(\alpha^2 + \beta^2)} \left(V_n(\mathbf{x}, t) - \int_{t_n}^t \rho(\mathbf{x}, \tau) d\tau \right) \right], \quad (3.11)$$

where

$$U_n(\mathbf{x}, t) = \frac{\exp [\eta V_n(\mathbf{x}, t)]}{1 + \eta |\psi(\mathbf{x}, t_n)|^2 \int_{t_n}^t \exp [\eta V_n(\mathbf{x}, \tau)] d\tau}. \quad (3.12)$$

Again, with $V(\mathbf{x}, t) = V_0(\mathbf{x})$, we can integrate exactly to get

$$\psi(\mathbf{x}, t) = \psi(\mathbf{x}, t_n) \begin{cases} \exp \left[\frac{i}{\varepsilon^2 \beta} (V_0(\mathbf{x}) - |\psi(\mathbf{x}, t_n)|^2) (t - t_n) \right], & \alpha = 0, \\ \sqrt{\hat{U}(\mathbf{x}, t)} \exp \left[\frac{i\beta}{2\alpha} \ln \hat{U}(\mathbf{x}, t) \right], & \alpha \neq 0, \end{cases} \quad (3.13)$$

where

$$\hat{U}(\mathbf{x}, t) = \begin{cases} \frac{1}{1 + \eta |\psi(\mathbf{x}, t_n)|^2 (t - t_n)}, & V_0(\mathbf{x}) = 0, \\ \frac{V_0(\mathbf{x})}{|\psi(\mathbf{x}, t_n)|^2 + (V_0(\mathbf{x}) - |\psi(\mathbf{x}, t_n)|^2) \exp(-\eta V_0(\mathbf{x})(t - t_n))}, & V_0(\mathbf{x}) \neq 0. \end{cases}$$

Remark 3.1. If the function $V_n(\mathbf{x}, t)$ as well as other integrals in (3.11) cannot be evaluated analytically, numerical quadrature can be used, for example,

$$V_n(\mathbf{x}, t_{n+1}) = \int_{t_n}^{t_{n+1}} V(\mathbf{x}, \tau) d\tau \approx \frac{\Delta t}{6} [V(\mathbf{x}, t_n) + 4V(\mathbf{x}, t_n + \Delta t/2) + V(\mathbf{x}, t_{n+1})].$$

Remark 3.2. In practice, we always use the second-order Strang splitting [45], that is, from time $t = t_n$ to $t = t_{n+1}$: (i) evolve (3.5) for half-time step $\Delta t/2$ with initial data given at $t = t_n$; (ii) evolve (3.4) for one time step Δt starting with the new data; and (iii), evolve (3.5) for half-time step $\Delta t/2$ with the newer data.

3.2 Discretization in space

To solve (3.4), we adopt the polar coordinate (r, θ) so as to match the highly oscillatory boundary condition (3.2) in the transverse direction, and try to formulate the equation in a variable-separable form. We discretize in θ -direction by the Fourier pseudo-spectral method, in r -direction by FEM and in time by Crank-Nicolson scheme. With the following

expansion

$$\psi(r, \theta, t) = \sum_{l=-L/2}^{l=L/2-1} \widehat{\psi}_l(r, t) e^{il\theta}, \tag{3.14}$$

where L is an even positive integer and $\widehat{\psi}_l(r, t)$ is the Fourier coefficient for the l -th mode, we can take (3.14) into (3.4) and get for $-\frac{L}{2} \leq l \leq \frac{L}{2} - 1$ and $0 < r < R$:

$$(\alpha - i\beta) \partial_t \widehat{\psi}_l(r, t) = \frac{1}{r} \frac{\partial}{\partial r} \left(r \frac{\partial \widehat{\psi}_l(r, t)}{\partial r} \right) - \frac{l^2}{r^2} \widehat{\psi}_l(r, t), \tag{3.15}$$

$$\widehat{\psi}_l(R, t) = \delta_{lm} \quad (\text{for all } l), \quad \widehat{\psi}_l(0, t) = 0 \quad (\text{for } l \neq 0); \tag{3.16}$$

where δ_{lm} is the Kronecker delta satisfying

$$\delta_{lm} = \begin{cases} 1 & l = m, \\ 0 & l \neq m. \end{cases}$$

Let P^k denote all polynomials with degree at most k , $J > 0$ be a chosen integer, $0 = r_0 < r_1 < r_2 < \dots < r_J = R$ be a partition for the interval $[0, R]$ with a mesh size $h = \max_{0 \leq j < J} \{r_{j+1} - r_j\}$. Define a finite element space by

$$U^h = \{u^h \in C[0, R] \mid u^h|_{[r_j, r_{j+1}]} \in P^k, 0 \leq j < J, u^h(R) = \delta_{lm}\},$$

for $l = 0$, and for $l \neq 0$,

$$U^h = \{u^h \in C[0, R] \mid u^h|_{[r_j, r_{j+1}]} \in P^k, 0 \leq j < J, u^h(0) = 0, u^h(R) = \delta_{lm}\},$$

then we obtain the FEM approximation for (3.15)–(3.16): Find $\widehat{\psi}_l^h(\cdot, t) \in U^h$ such that for all $\varphi^h \in U^h$ and $t_n \leq t \leq t_{n+1}$,

$$(\alpha - i\beta) \frac{d}{dt} A(\widehat{\psi}_l^h(\cdot, t), \varphi^h) = B(\widehat{\psi}_l^h(\cdot, t), \varphi^h) + l^2 C(\widehat{\psi}_l^h(\cdot, t), \varphi^h), \tag{3.17}$$

where for $u^h, v^h \in U^h$,

$$\begin{aligned} A(u^h, v^h) &= \int_0^R r u^h(r) v^h(r) dr, & B(u^h, v^h) &= - \int_0^R r \frac{du^h(r)}{dr} \frac{dv^h(r)}{dr} dr, \\ C(u^h, v^h) &= - \int_0^R \frac{1}{r} u^h(r) v^h(r) dr. \end{aligned}$$

The ODE system (3.17) is then discretized by the standard Crank-Nicolson scheme in time. Although an implicit time discretization is applied for (3.17), the one-dimensional nature of the problem makes the coefficient matrix for the linear system band limited. For example, if the piecewise linear polynomial is used, that is, $k = 1$ in U^h , the matrix is tridiagonal. Fast algorithms can be applied to solve the resulting linear systems.

For the discretization considered here, the total memory requirement is $O(JL)$ and the total computational cost per time step is $O(JL \ln L)$.

Remark 3.3. As noticed in [4, 30], (3.15)–(3.16) may also be discretized using the finite difference in space on a mesh with a shifted grid and the Crank-Nicolson scheme in time. When the standard second-/fourth-order finite difference is applied in space, only a tridiagonal/pentadiagonal linear system needs to be solved, which can be done via $O(J)$ arithmetic operations, see Bao *et al.* [4] for details.

4 Simulations of quantized vortices

In this section, we apply the numerical method described in the previous section to study, in the context of GLSE (1.1)–(1.3), the stability of central vortex states with different winding numbers, the interaction of two vortices with winding number $m = \pm 1$, the dynamics of vortex lattices and the vortex motion with inhomogeneous external potential. These are documented in different subsections. Wherever simulation results are given, some discussions are made on the basis of the numerical findings. All simulation results are justified and confirmed numerically by using a finer mesh and a smaller time step.

For all the simulations, we in general report results for three separate cases:

Case I. Ginzburg-Landau equation (GLE): $\alpha = 1, \beta = 0$ in (1.1);

Case II. Nonlinear Schrödinger equation (NLSE): $\alpha = 0, \beta = 1$ in (1.1);

Case III. Complex Ginzburg-Landau equation (CGLE): $\alpha = 1, \beta = 1$ in (1.1).

Notice that the computation in Case II is often the most difficult one due to the dispersive nature of the NLSE and there are very few conclusive simulation results in such a case.

In our computation, we take $R = 7,400$ for Ω_R and time step $\Delta t = 0.0001$. In θ -direction, a uniform mesh with mesh size $\Delta\theta = \pi/128$, that is, $L = 256$ in (3.14), is used. In r -direction, a graded piecewise uniform mesh with 6,001 grid points from the smallest mesh size $\Delta r = 1/60$ for the subinterval $[0, 10]$ to the largest mesh size $\Delta r = 11/3$ for the subinterval $[6, 300, 7, 400]$ is applied. These parameter values have been tested to ensure the accuracy of the simulation results.

4.1 Stability of vortex states

To study the stability of vortex states of the GLSE numerically, we take $\varepsilon = 1$ and $V_0(\mathbf{x}) \equiv 1$ in (1.1) and choose the initial data (3.3) as

$$\psi_0(\mathbf{x}) = \phi_m(\mathbf{x}) = f_m(r)e^{im\theta}, \quad \mathbf{x} \in \Omega_R,$$

where $f_m(r)$ is the numerical solution of (2.4)–(2.5), as depicted in Figure 1.

As it is commonly accepted that the stability of vortices is dependent on the type of perturbations, we thus consider two types of perturbations in the following:

Type 1. Small perturbation on the initial data; an example is given by artificially setting $\psi_0(\pm 0.2, 0) = 0$ and choosing $W(\mathbf{x}, t) \equiv 0$ in (3.1).

Type 2. Perturbation on the external potential; an example is given by introducing a far-blue detuned Gaussian laser beam stirrer with height $W_s(t)$, width w_s and at

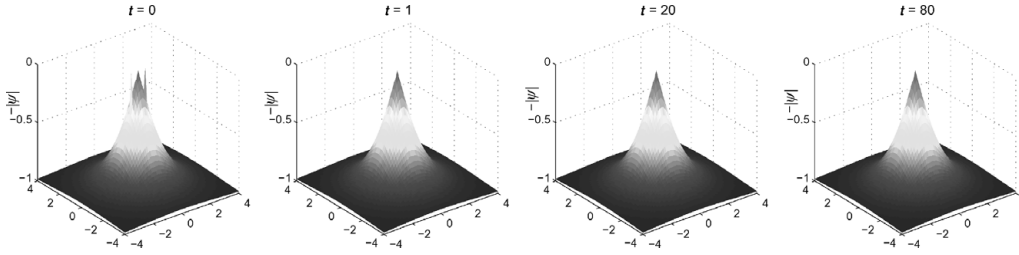


FIGURE 2. Surface plots of $-\psi(\mathbf{x}, t)$ at different times for the stability study of the vortex state ($m = 1$) in GLE under Type 1 perturbation.

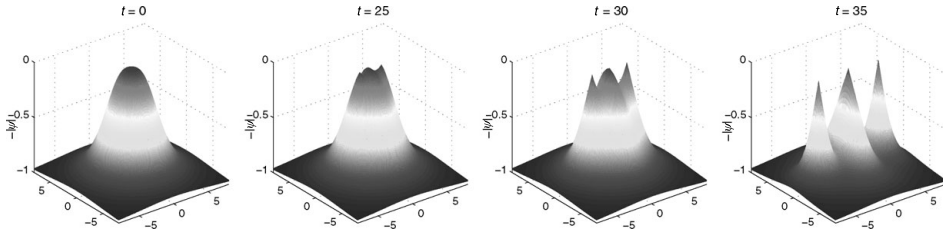


FIGURE 3. Surface plots of $-\psi(\mathbf{x}, t)$ at different times for the stability study of the vortex state ($m = 3$) in GLE under Type 1 perturbation.

position $\mathbf{x}_s(t)$:

$$W(\mathbf{x}, t) = W_s(t) \exp \left[- \left(\frac{|\mathbf{x} - \mathbf{x}_s(t)|^2}{w_s/2} \right) \right]. \tag{4.1}$$

The numerical results corresponding to the GLE under a perturbation on the initial data, that is, type 1, are illustrated in Figures 2 and 3.

For vortex states with different winding numbers ($m = 1$ and $m = 3$ separately), the figures illustrate their stability under this type of perturbations. Note that, for more clear illustration of the vortices, the displays given in the figures often only portray the solutions on a small portion of the much bigger spatial computational domain. Such a practice is also applied to figures given in this article, though the portions where the solutions are shown often vary in order to most effectively capture the interesting properties of the solutions.

In comparison, Figures 4 and 5 show similar results for the NLSE under a perturbation on the external potential, that is, Type 2. In addition, Figures 6 and 7 present the trajectories of vortex centres and the radiation for the same stability study of a vortex state ($m = 2$) in the NLSE. In our implementation, the parameters in (4.1) are chosen as $w_s = 1$, and

$$(x_s(t), y_s(t)) \equiv (3, 0), \quad W_s(t) = \begin{cases} -5 \sin^2(2t), & t \in [0, \pi/2], \\ 0, & t \geq \pi/2. \end{cases}$$

Thus, the perturber is only introduced when $t \in [0, \pi/2]$, and when $t \geq \pi/2$, it is removed.

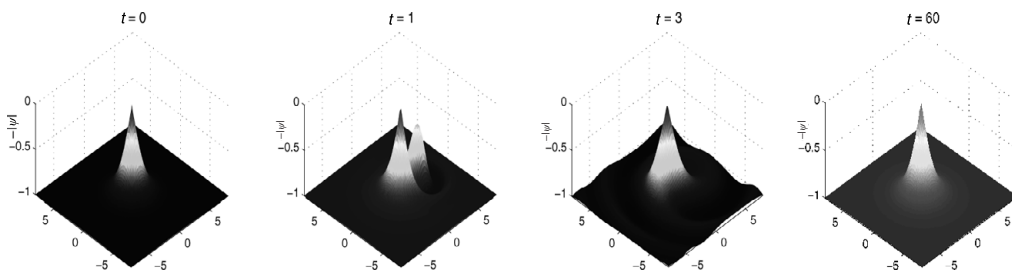


FIGURE 4. Surface plots of $-\psi(\mathbf{x}, t)$ at different times for the stability study of the vortex state ($m=1$) in NLSE under Type 2 perturbation.

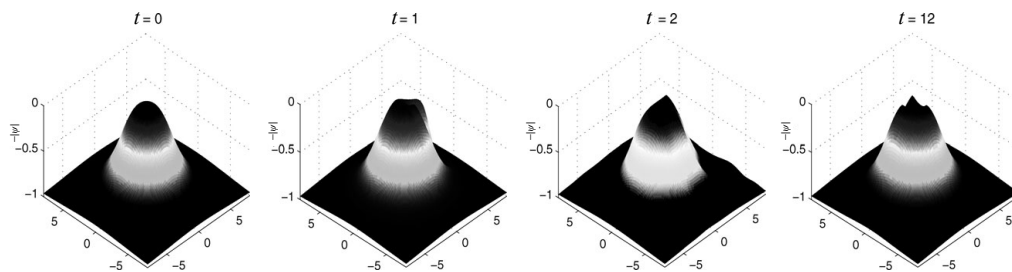


FIGURE 5. Surface plots of $-\psi(\mathbf{x}, t)$ at different times for the stability study of the vortex state ($m=3$) in the NLSE under Type 2 perturbation.

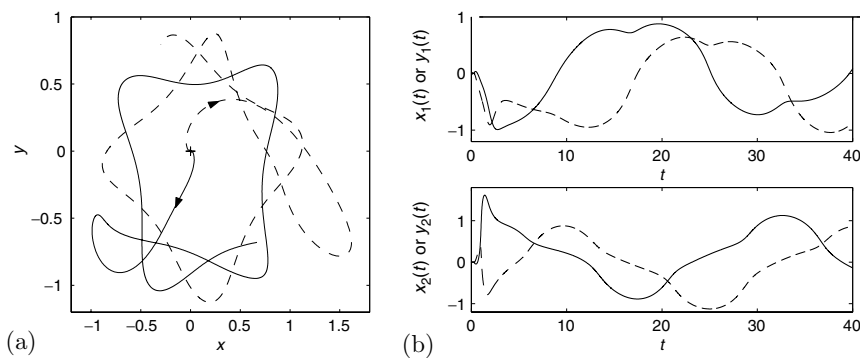


FIGURE 6. Dynamics of the vortex centres for the stability study of the vortex state with $m=2$ in the NLSE under a Type 2 perturbation; (a) trajectory; (b) time evolution (solid line: $x(t)$; dashed line: $y(t)$).

From Figures 2–7 and similar numerical experiments for other index m (omitted here for brevity), we may draw the following conclusions for the stability of vortex states in the GLSE, depending on the winding numbers.

Firstly, the vortex states with winding number $m=\pm 1$ are dynamically stable in all three cases, that is, in the GLE, NLSE and CGLE (cf. Figures 2 and 4). This substantiates

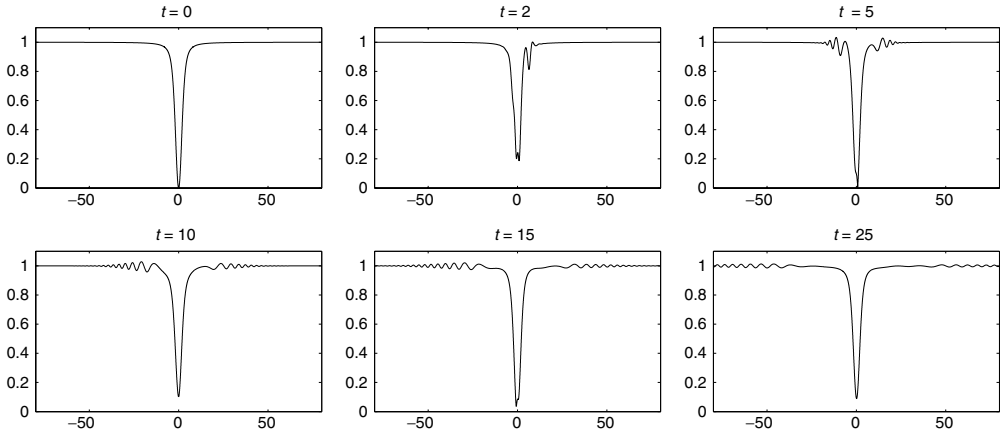


FIGURE 7. Plots of $|\psi(x, 0, t)|$ at different times for the stability study of the vortex state with $m = 2$ in the NLSE under a Type 2 perturbation.

the stability assumption used in the studies of such vortex dynamics in the literature for the GLE and NLSE [35].

Secondly, for the vortex states with winding number $|m| > 1$, there are two different scenarios. On one hand, for the GLE and CGLE, they are dynamically unstable under perturbations that are either in the initial data or in the external potential (cf. Figure 3). When t is large, a vortex state initially with winding number m splits into $|m|$ well-separated vortices with winding number $+1$ when $m > 0$ and -1 when $m < 0$, respectively. The details of the splitting and the motion of the $|m|$ separated vortex centres depend on the perturbation. These results very well agree with those for the GLE in the literature [22, 36]. On the other hand, for the NLSE, these vortex states with winding number $|m| > 1$ are dynamically stable under a small perturbation in the initial data, but unstable under a perturbation in the external potential (cf. Figure 5). In the latter case, a vortex state with a winding number m will split into $|m|$ vortices, though the core of $|m|$ vortices are well overlapped (cf. Figure 5). We also conducted some studies on the effect of radiation for this set of experiments. It was predicted that, for example, in Lange and Schroers [31], a perturbed vortex configuration for the NLSE with $m = 2$ would rotate (cf. Figure 6) and would also emit radiation (cf. Figure 7), which carries away energy. The small oscillations observed in Figure 7 correspond to sound waves generated in the dynamics, which is justified numerically by using different finer meshes and smaller time steps. The vortex configuration would then make adjustment by finding a configuration of lower energy, that is to say, by splitting up into two $m = 1$ vortices (cf. Figure 6). It is unclear which type of perturbation is implied in Lange and Schroers [31], but the above prediction is nevertheless consistent with our simulation using a perturbation in the external potential (cf. Figures 6 and 7).

4.2 Interaction of two vortices with winding number $m = \pm 1$

Since a vortex state with winding number $m = \pm 1$ is dynamically stable in the GLSE (1.1), it is thus of interest to study their dynamic interactions. To do so, we take $\varepsilon = 1$ and

$V_0(\mathbf{x}) \equiv 1$ in (1.1) and choose the initial data (3.3) as

$$\psi_0(\mathbf{x}) = \phi_{m_1}(\mathbf{x} - \mathbf{x}_1^0)\phi_{m_2}(\mathbf{x} - \mathbf{x}_2^0) = \phi_{m_1}(x - x_1^0, y - y_1^0)\phi_{m_2}(x - x_2^0, y - y_2^0), \quad (4.2)$$

where ϕ_{m_j} is the vortex state given by (2.3) with winding number m_j ($m_j = 1$ or -1). That is, we want to study the interaction of two vortices with initial centres at $\mathbf{x}_j^0 = (x_j^0, y_j^0)$ ($j = 1, 2$). We take $m = m_1 + m_2$ in (3.2) and refer to the vortex with $m_j = 1$ as having a positive charge, while $m_j = -1$ as a negative charge.

Here, we study numerically two cases of interaction by solving the GLSE (3.1) with initial data (4.2) involving two vortices, using the method discussed in the previous section:

Case I. Two vortices with like winding numbers, that is, $m_1 = m_2 = 1$, $\mathbf{x}_1^0 = (a, 0)$ and $\mathbf{x}_2^0 = (-a, 0)$ with a constant;

Case II. Two vortices with opposite winding numbers, that is, $m_1 = -m_2 = 1$, $\mathbf{x}_1^0 = (a, 0)$ and $\mathbf{x}_2^0 = (-a, 0)$ with a constant.

Figure 8 gives the time evolution of vortex centres for Case I, and Figure 9 presents similar results for Case II. Furthermore, Figure 10 shows the time evolution of the rescaled free energy $E(\psi)$.

From Figures 8–10, we can draw the following conclusions for the interaction of two vortices described by the GLSE (1.1):

First of all, for the GLE, two vortices with like (opposite) winding numbers undergo a repulsive (attractive) interaction, and the centres of the two vortices move along a straight line passing through their locations at $t = 0$ (cf. Figures 8(a) and 9(a)) with their speeds depending on their distance. The larger is the distance, the slower is the motion. One can compare this with the reduced dynamics of vortex centres [36, 39] in the GLE. One can easily deduce that if we start with two like vortices in symmetric locations $\pm(a, 0)$, then the solution of the reduced dynamics [36, 39] is given by $\pm(\sqrt{a^2 + \kappa_l t}, 0)$, with κ_l as a constant. On the other hand, with two opposite vortices, the solution of the reduced dynamics [36] is given by $\pm(\sqrt{a^2 - \kappa_o t}, 0)$ before the annihilation, with κ_o as a constant, which implies the collision time $T_c = a^2/\kappa_o = O(a^2)$. Their conclusions are consistent with our numerical simulations. In addition, as expected, the rescaled free energy decreases in the GLE (cf. Figure 10(a)). Furthermore, for two vortices with opposite winding numbers, the energy almost decreases to zero during the collision (cf. Figure 10(b)).

Secondly, for NLSE, vortices behave like point vortices in an ideal fluid. If the two vortices have the same winding number (charge) with initial distance $d_0 = |\mathbf{x}_1^0 - \mathbf{x}_2^0| = 2a$, there exists a critical time $t_0 > 0$, depending on d_0 , such that before time t_0 , that is, $0 \leq t \leq t_0$, the two vortices move from their initial locations to a circle with diameter $d_1 = |\mathbf{x}_1(t_0) - \mathbf{x}_2(t_0)|$ and the change of the distance between the two vortex centres is rapid (cf. Figure 8(c)); after time t_0 , that is, for $t \geq t_0$, the two vortices rotate along a circle (counterclockwise when winding number $m_j = +1$ and clockwise when $m_j = -1$ respectively), like a spin with an angular frequency $\omega(d_0)$, and the diameter of the circle increases very slowly. Our numerical results here suggest that the reduced dynamics [36, 38] of vortex centres in the NLSE in this case is qualitatively correct (cf. Figure 8(c)) when $d_0 = 2a$ is large, and corrections must be added when d_0 is small.

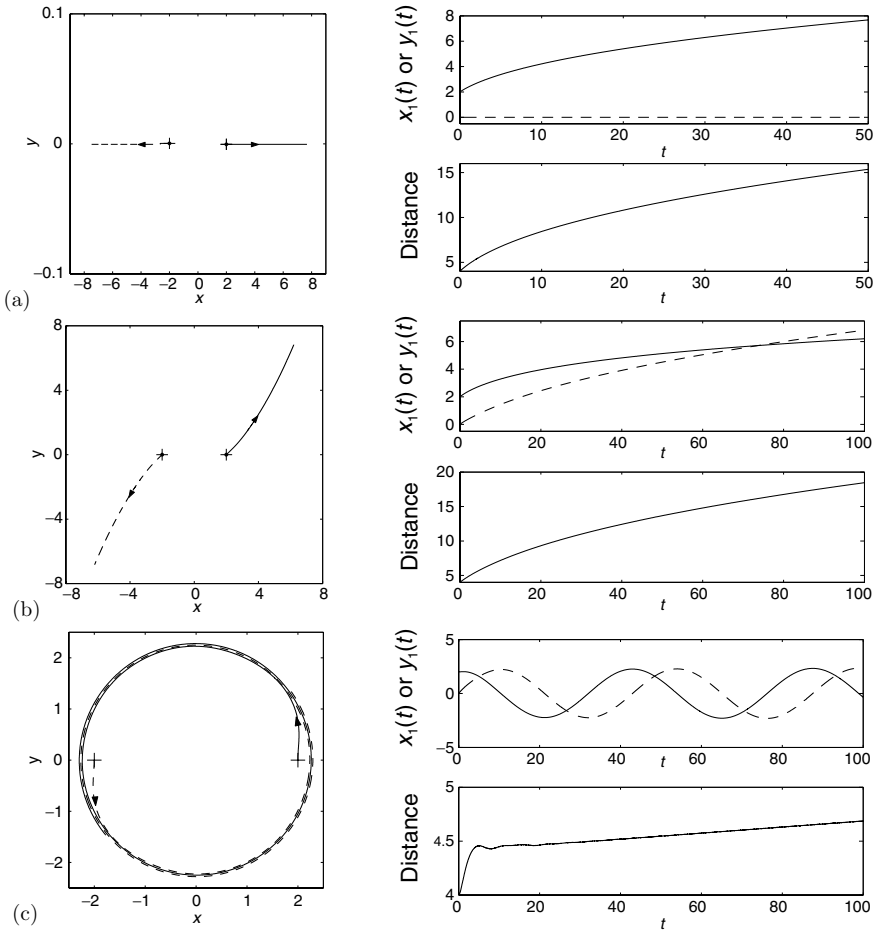


FIGURE 8. Time evolution of vortex centres for Case I with $a = 2$. (a) GLE; (b) CGLE; (c) NLSE.

On the other hand, for the case of two vortices having opposite charge, there is a critical distance d_{cr} satisfying that, for $d_0 = |\mathbf{x}_1^0 - \mathbf{x}_2^0| < d_{cr}$, the two vortices approach each other while drifting sideways and then collapse to annihilate each other (cf. Figure 9(c)); and for $d_0 = |\mathbf{x}_1^0 - \mathbf{x}_2^0| > d_{cr}$, they move almost in parallel (cf. Figure 9(e)). Our simulations suggest that $d_{cr} \approx 2r_1^0 = 2 \times 1.75 = 3.5$, that is, two times of the core size r_1^0 , which is almost three times the theoretical prediction $d_{cr} \approx \sqrt{2}$ [40]. Thus, our numerical experiments provide very precise characterisation on the range of validity of the reduced dynamics [36, 39] in terms of the separation length between the opposite vortices. Also, we note for the NLSE dynamics, the rescaled free energy is conserved during time evolution in the two cases (cf. Figure 10).

Next, for the case of CGLE, two vortices with the same charge move away from each other and the trajectory is a combination of a straight line and a circle (cf. Figure 8(b)). On the contrary, two vortices with opposite charges collide after some time (cf. Figure 9(b)).

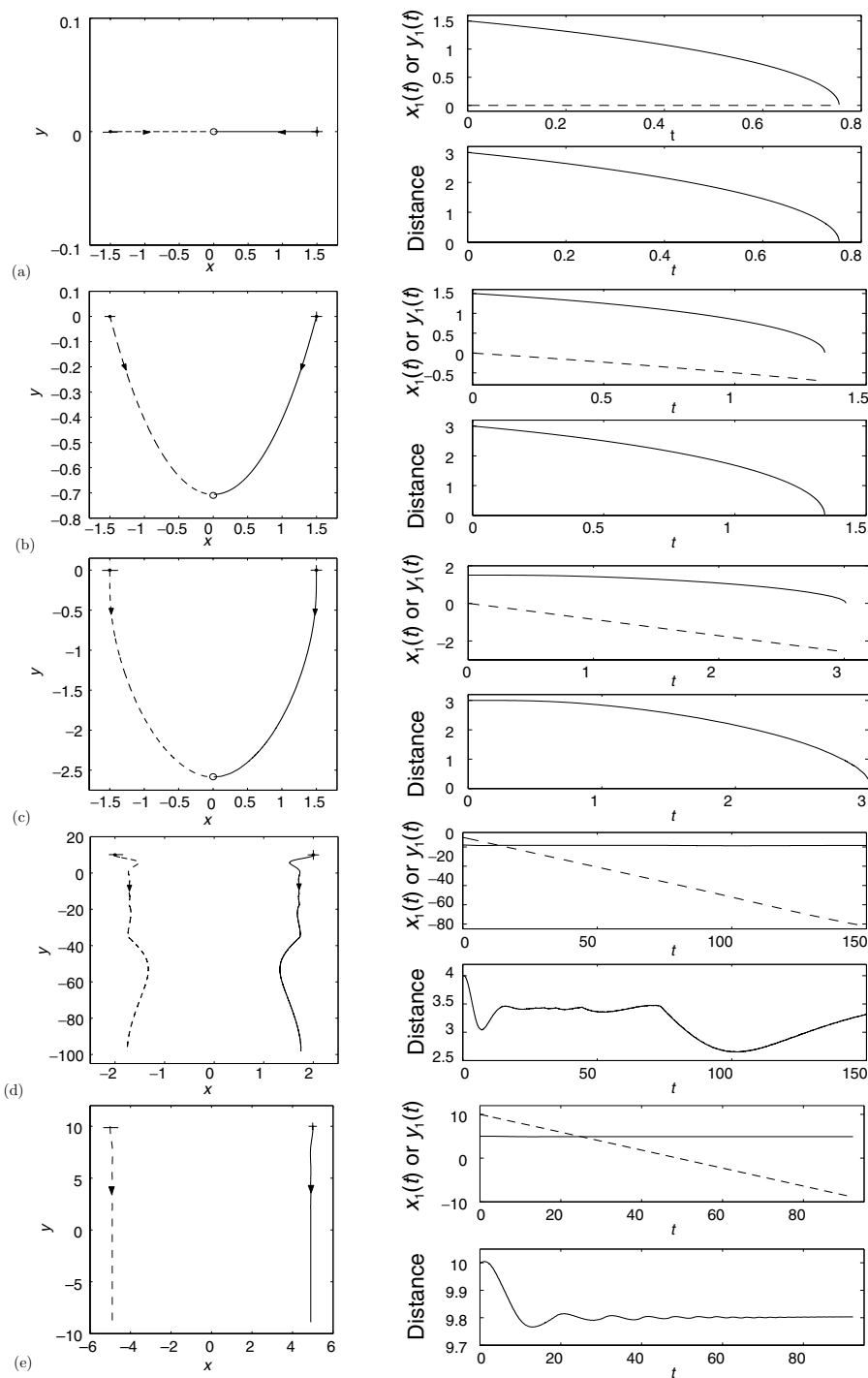


FIGURE 9. Time evolution of vortex centres for Case II. (a) GLE with $a = 1.5$; (b) CGLE with $a = 1.5$; (c) NLSE with $a = 1.5 < r_1^0 \approx 1.75$; (d) NLSE with $a = 2 > r_1^0$; and (e) NLSE with $a = 5 \gg r_1^0$.

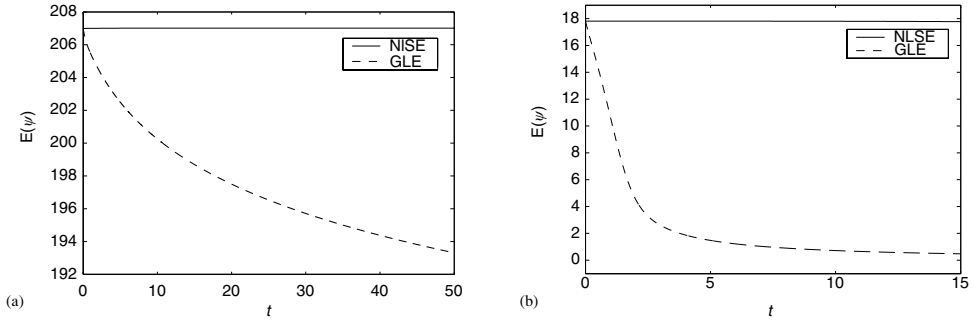


FIGURE 10. Time evolution of the rescaled *free energy* $E(\psi)$ with $a = 2$. (a) Case I; (b) Case II.

4.3 Dynamics of vortex lattices

In this subsection, we present numerical studies on the dynamics of vortex lattices in the GLSE (1.1). We take $\varepsilon = 1$ and $V_0(\mathbf{x}) \equiv 1$ in (1.1) and choose the initial data (3.3) as

$$\psi_0(\mathbf{x}) = \prod_{j=1}^N \phi_1(\mathbf{x} - \mathbf{x}_j^0) = \prod_{j=1}^N \phi_1(x - x_j^0, y - y_j^0), \quad (4.3)$$

where N is the total number of vortices in the lattice and ϕ_1 is the vortex state given by (2.3) with winding number $m_j = 1$. We take $m = N$ in (3.2) and study two cases:

Case I. $N = 9$ and the initial vortex centres are located on a uniform 3×3 mesh points for the rectangle $[-4, 4] \times [-4, 4]$;

Case II. $N = 25$ and the initial vortex centres are located on a uniform 5×5 mesh points for the rectangle $[-4, 4] \times [-4, 4]$;

Figures 11 and 12 show the surface plots of $-|\psi|$ and the time evolution of vortex centres for Case I in the GLE and the NLSE, respectively. Figure 13 shows $|\psi(x, 0, t)|$ ($x \geq 0$) at different times for the NLSE in Case I, while Figure 14 shows the contour plots of $|\psi|$ for the NLSE in Case II.

On the basis of Figures 11 to 14, we can draw the following conclusions. Firstly, for the GLE and NLSE, the vortex initially at the origin does not move because of the symmetry (cf. Figures 11(a)–(b), 12(a)–(b) and 14). Secondly, for the GLE in Case I, each vortex centre moves outward along the line passing through its location at $t = 0$ and the origin (cf. Figure 11(b)). After some time, the lattice splits into nine well-separate vortex states with winding number $m_j = 1$ (cf. Figure 11(a)). At any time t , the four vortices initially located at the four corners of the lattice are always on a circle with radius $r_1(t)$; and the other four vortices initially located at the axes of the lattice are always on another circle with radius $r_2(t)$. The radii of the two circles, that is, $r_1(t)$ and $r_2(t)$, increase when the time t increases, but their distance, that is, $|r_1(t) - r_2(t)|$, decreases when t increases (cf. Figure 11(c)). Thirdly, for the NLSE, the vortices rotate counterclockwise and move along two circles. The distance between the two circles changes periodically (cf. Figure 12(c)). The vortex cores are well overlapped for a very long time. During the time evolution, sound waves are generated and they radiate outward in the NLSE (cf. Figure 13).

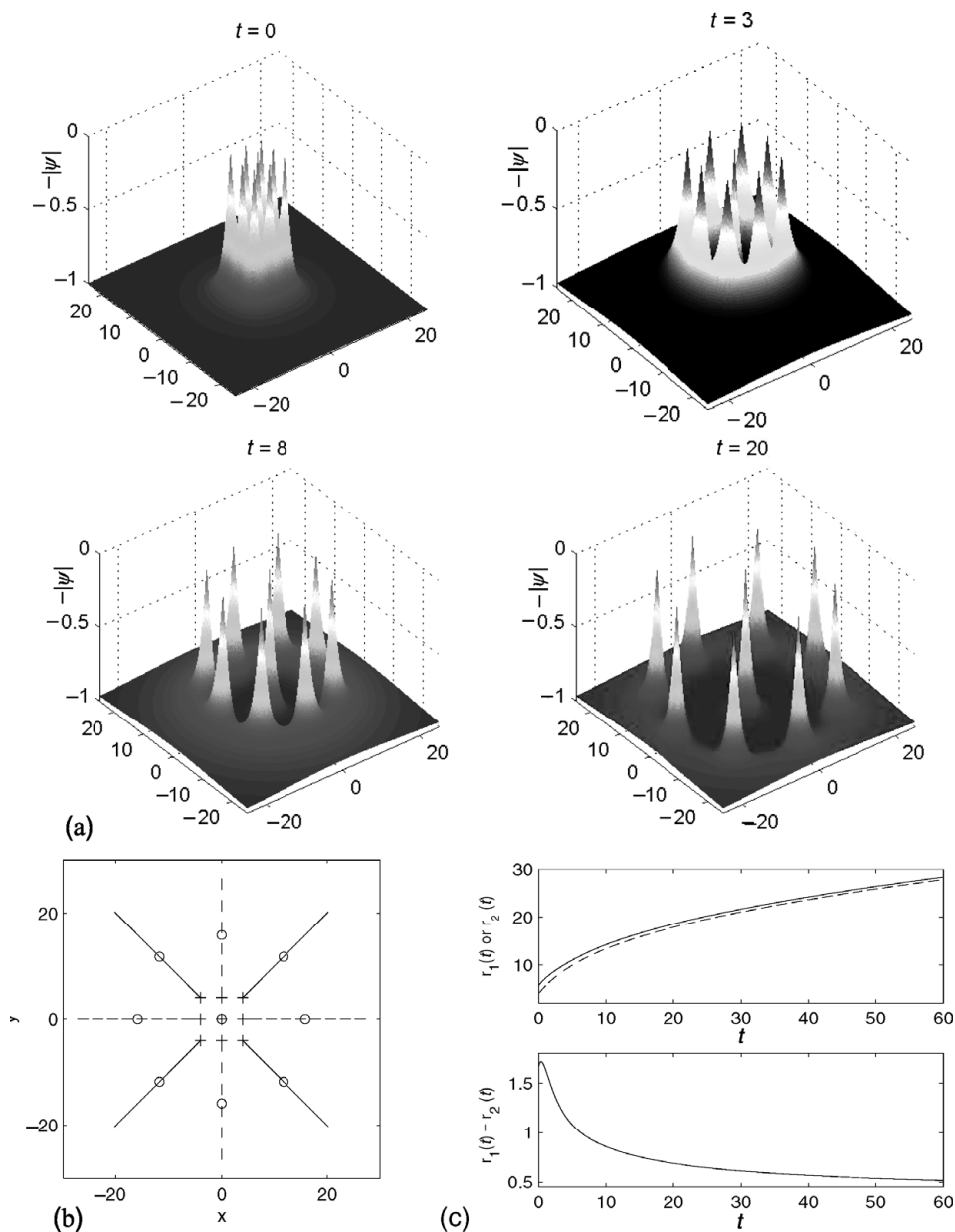


FIGURE 11. (a) Surface plots of $-\lvert\psi\rvert$ at different times; (b) trajectory of the vortex centres (‘+’: $t = 0$ and ‘o’: $t = 15$); and (c) time evolution of vortex centres, for dynamics of a vortex lattice with nine vortices (Case I) for the GLE.

4.4 Dynamics of vortex under inhomogeneous external potential

In this subsection, we numerically study the dynamics of vortices under an inhomogeneous external potential. We take $V_0(\mathbf{x})$ in (1.1) as

$$V_0(\mathbf{x}) = \frac{1}{1 + e^{-(\gamma_x x^2 + \gamma_y y^2)}} = \frac{1}{1 + e^{-r^2(\gamma_x \cos^2 \theta + \gamma_y \sin^2 \theta)}}, \quad \mathbf{x} \in \mathbb{R}^2, \quad (4.4)$$

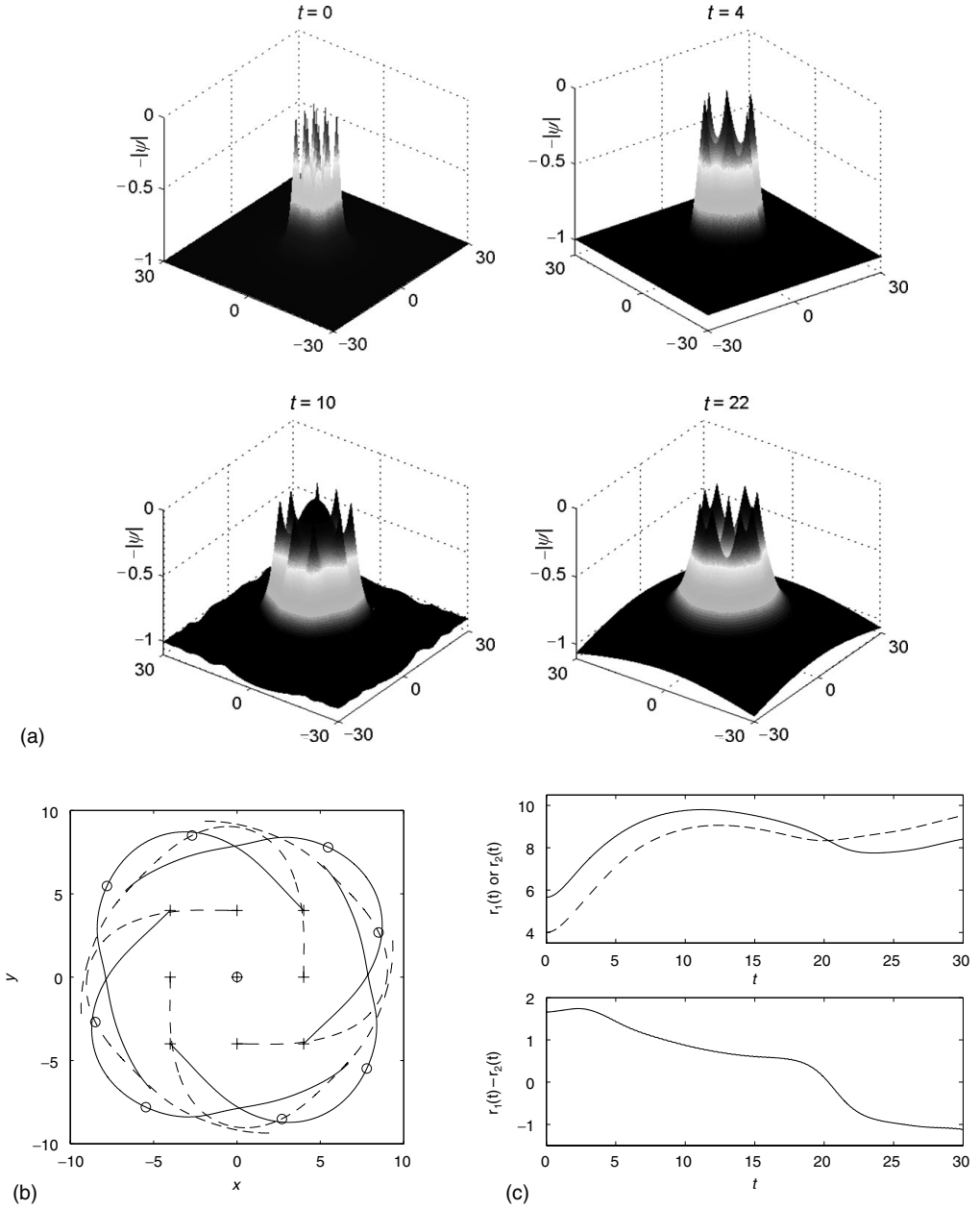


FIGURE 12. (a) Surface plots of $-\psi$ at different times; (b) trajectory of the vortex centres ('+': $t = 0$ and 'o': $t = 15$); and (c) time evolution of vortex centres, for dynamics of a vortex lattice with nine vortices (Case I) for the NLSE.

where γ_x and γ_y are two positive constants. It is easy to see that $V_0(\mathbf{x})$ attains its minimum value $1/2$ at the origin. The initial data are chosen as

$$\psi(\mathbf{x}, 0) = \psi_0(\mathbf{x}) = \phi_1(\mathbf{x} - \mathbf{x}^0), \quad \mathbf{x} \in \mathbb{R}^2, \tag{4.5}$$

where $\phi_1(\mathbf{x})$ is the vortex state of (2.1)–(2.2) with winding number $m = 1$.

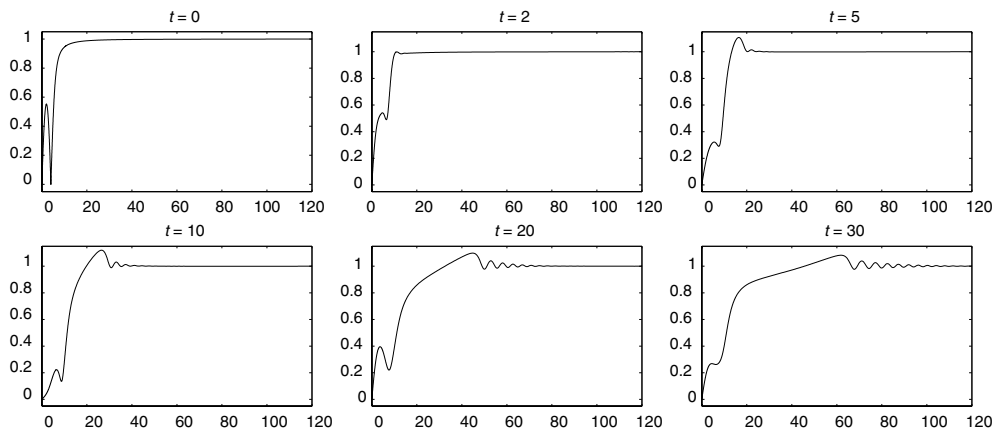


FIGURE 13. Plots of $|\psi(x, 0, t)|$ ($x \geq 0$) at different times for the NLSE in Case I for showing sound wave propagation.

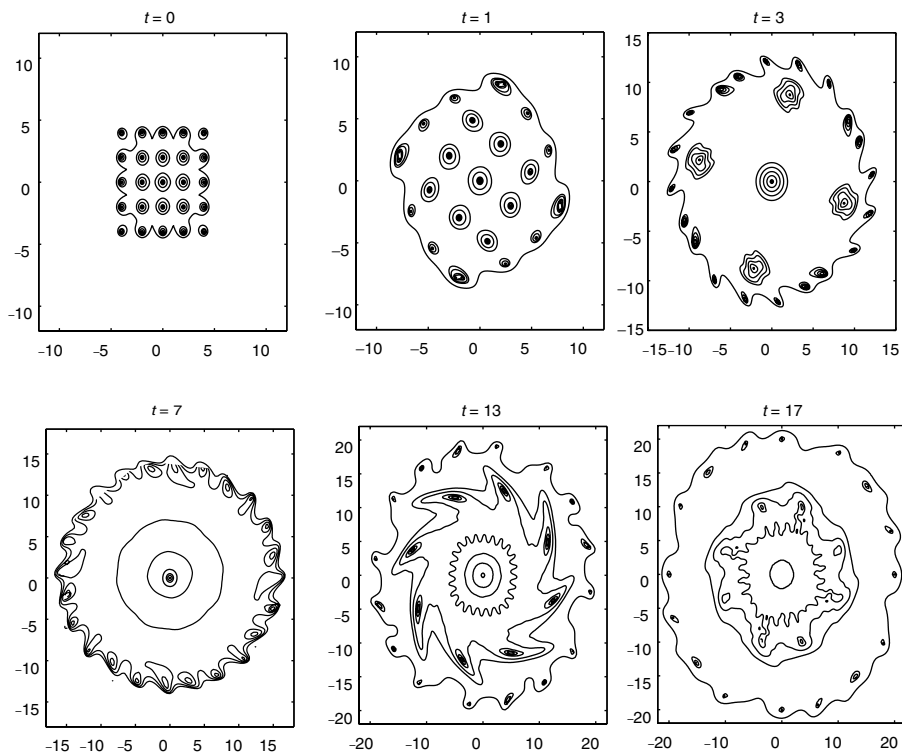


FIGURE 14. Contour plots of $|\psi|$ at different times for dynamics of the NLSE with 25 vortices (Case II).

We now study the dynamics of vortex under two types of inhomogeneous external potential:

Case I. Symmetric external potential, that is, $\gamma_x = \gamma_y = 1$ in (4.4);

Case II. Anisotropic external potential, that is, $\gamma_x = 1$ and $\gamma_y = 20$ in (4.4).

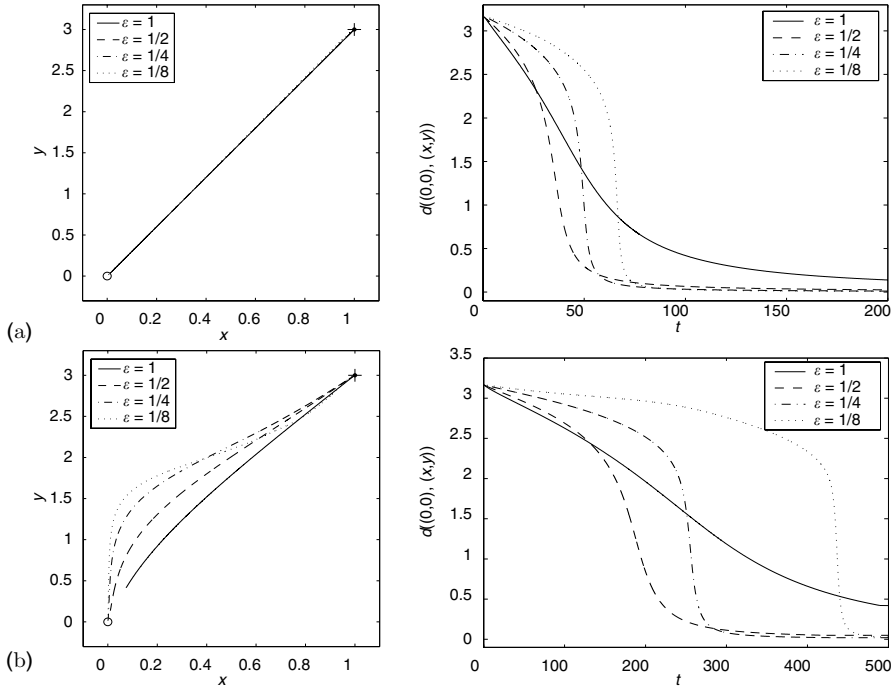


FIGURE 15. Vortex centre trajectory (left) and its distance to the origin (right) under an inhomogeneous external potential for the GLE: (a) Case I; (b) Case II.

Dynamically, for the GLE, that is, $\beta = 0$ in (1.1), one can compute analytically the velocity of the induced motion due to the inhomogeneous impurities as follows [26]:

$$\mathbf{v}(t) := \frac{d\mathbf{x}(t)}{dt} = -\nabla \ln V_0(\mathbf{x}(t)) = 2 [V_0(\mathbf{x}(t)) - 1] G\mathbf{x}(t), \quad \text{where } G = \begin{pmatrix} \gamma_x & 0 \\ 0 & \gamma_y \end{pmatrix},$$

with $\mathbf{x}(0) = \mathbf{x}^0$. In this approximate vortex dynamic law of the GLE with impurity, the vortex will move to the minimizer of the external potential $V_0(\mathbf{x})$. Furthermore, in Case I, the trajectory is a segment connected to \mathbf{x}^0 and the minimizer of $V_0(\mathbf{x})$. For the NLSE and CGLE, the dynamic laws with impurities remain to be established.

Figures 15–16 show the trajectory of the vortex centre with $\mathbf{x}^0 = (1, 3)$ in (4.5) for the GLE and CGLE with different values of ε . Figure 17 shows similar results for the NLSE with $\mathbf{x}^0 = (1, 2)$.

From Figures 15 and 17, we can draw the following conclusions. Firstly, for the GLE and CGLE, the vortex centre moves monotonically to the position where the external potential $V_0(\mathbf{x})$ attains its minimum value (cf. Figures 15 and 16), illustrating the pinning effect. The speed of the motion depends on the values of the parameter ε . The trajectory of the vortex centre depends on the external potential $V_0(\mathbf{x})$, which agrees with the reported analytical results for the GLE [25, 26, 34]. Secondly, for the NLSE, the vortex centre moves rotationally clockwise to the minimum position of the external potential

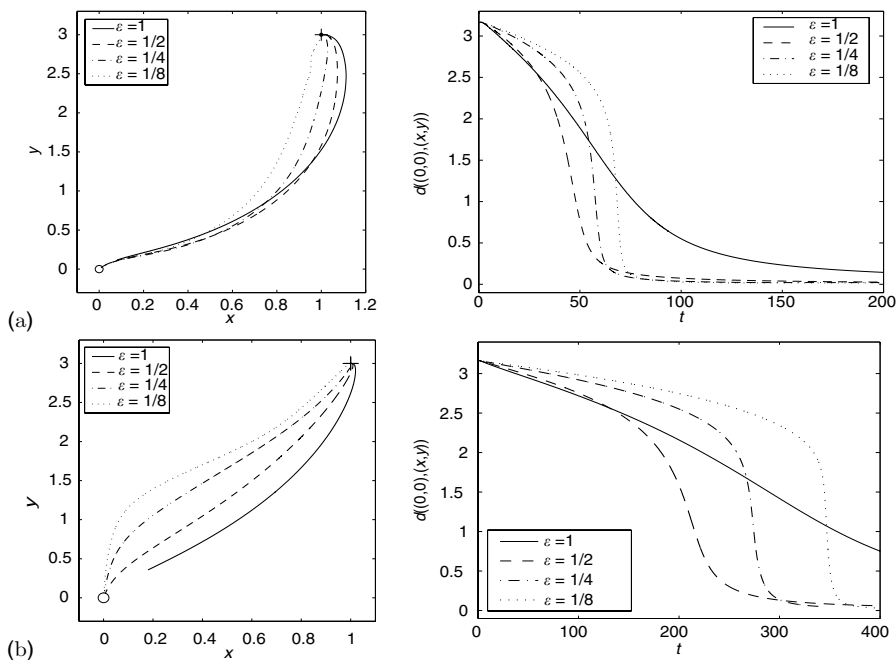


FIGURE 16. Vortex centre trajectory (left) and its distance to the origin (right) under an inhomogeneous external potential for the CGLE: (a) Case I; (b) Case II.

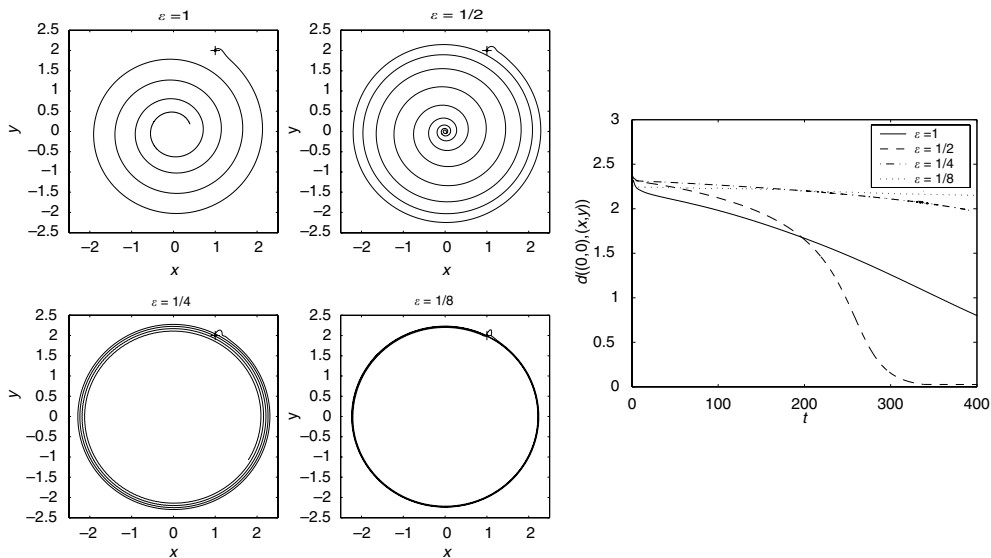


FIGURE 17. Vortex centre trajectory (left) and its distances to the origin (right) under an inhomogeneous external potential for the NLSE: Case I.

(cf. Figure 17). When ε is small, the smaller the ε is, the longer time the vortex centre stays on a circle. Additional experiments were carried out for Case II. Similar motion patterns are observed so the pictures are omitted here. Rigorous justification of this observation is still not available.

5 Conclusion

There have been extensive studies in recent years concerning the quantized vortex dynamics governed by the GLSE, yet many interesting questions remain open. By proposing an efficient, accurate and unconditionally stable numerical method for the GLSE with non-zero far-field conditions in two dimensions, and applying this new numerical method to the GLSE, we numerically examined issues such as the stability of quantized vortex, interaction of two vortices, dynamics of the quantized vortex lattice and motion of vortex under inhomogeneous external potential in the GLSE. We provided convincing numerical results to show that, for the real-time dynamics, the central vortex state are dynamically stable only for the one with index (or winding number) $m = \pm 1$ in the GLSE. We numerically verified that (i) in the case of the GLE, two vortices with like (opposite) winding numbers undergo a repulsive (attractive) interaction; (ii) in the case of NLSE, vortices behave like point vortices in ideal fluid; if two vortices have the same winding numbers, they move along a circle; and if they have the opposite winding numbers, they collide when their initial distance is small and move in parallel when their initial distance is large enough; (iii) in the presence of an inhomogeneous external potential, the vortex centre will move to the point where the external potential attains its minimum when time t is large enough; and (iv) sound wave is observed in the vortex dynamics of the NLSE. Furthermore, we also carried out a detailed simulation of the NLSE dynamics of vortex lattice with 25 vortices, which is extremely challenging computationally and is the first one available in the literature. Finally, the efficient, unconditionally stable and accurate numerical method can be applied to study quantized vortex interactions in the GLSE with different initial set-ups, and comparisons to the solutions of the reduced dynamics [26, 35, 36, 39] of the GLSE are reported [49]. In addition, we point out that the numerical method discussed here can be extended to study the dynamics and the interaction of vortex line states in three dimensions as well as in bounded domains for the GLSE.

Acknowledgements

We acknowledge support from the National University of Singapore grant No. R-146-000-081-112, from NSF-DMS 0409297 and from NSF-ITR 0205232. We also acknowledge Professors Fanghua Lin, Huaiyu Jian and Shi Jin for helpful discussions on the subject. The work was partially done while the last two authors were visiting the Institute for Mathematical Sciences, National University of Singapore, in 2005 through the support of the institute.

References

- [1] ADLER, S. & PIRAN, T. (1984) Relaxation methods for gauge field equilibrium equations. *Rev. Mod. Phys.*, **56**, 1–40.

- [2] ARANSON, I. & KRAMER, L. (2002) The world of the complex Ginzburg-Landau equation. *Rev. Mod. Phys.* **74**, 99–133.
- [3] BAO, W. (2004) Numerical methods for the nonlinear Schrödinger equation with nonzero far-field conditions. *Methods Appl. Anal.*, **11**, 367–388.
- [4] BAO, W., DU, Q. & ZHANG, Y. (2006) Dynamics of rotating Bose-Einstein condensates and their efficient and accurate numerical computation. *SIAM J. Appl. Math.*, **66**, 758–786.
- [5] BAO, W. & JAKSCH, D. (2003) An explicit unconditionally stable numerical methods for solving damped nonlinear Schrodinger equations with a focusing nonlinearity. *SIAM J. Numer. Anal.*, **41**, 1406–1426.
- [6] BAO, W., JAKSCH, D. & MARKOWICH, P. A. (2003) Numerical solution of the Gross-Pitaevskii Equation for Bose-Einstein condensation. *J. Comput. Phys.*, **187**, 318–342.
- [7] BAO, W., JIN, S. & MARKOWICH, P. A. (2002) On time-splitting spectral approximations for the Schrödinger equation in the semiclassical regime, *J. Comput. Phys.*, **175**, 487–524.
- [8] BAO, W., JIN, S. & MARKOWICH, P. A. (2003) Numerical study of time-splitting spectral discretizations of nonlinear Schrödinger equations in the semi-classical regimes. *SIAM J. Sci. Comp.* **25**, 27–64.
- [9] BAO, W. & ZHANG, Y. (2005) Dynamics of the ground state and central vortex states in Bose-Einstein condensation. *Math. Mod. Meth. Appl. Sci.* **15**, 1863–1896.
- [10] BESSE, C., BIDEGARAY, B. & DESCOMBES, S. (2002) Order estimates in time of splitting methods for the nonlinear Schrödinger equation. *SIAM J. Numer. Anal.* **40**, 26–40.
- [11] CHAPMAN, J. & RICHARDSON, G. (1995) Motion of vortices in type-II superconductors. *SIAM J. Appl. Math.* **55**, 1275–1296.
- [12] CHEN, X. F., ELLIOTT, C. M. & TANG, Q. (1994) Shooting method for vortex solutions of a complex-valued Ginzburg-Landau equation. *Proc. R. Soc. Edinb. A—Math.* **124**, 1075–1088.
- [13] CHEN, Z. & DAL, S. (2001) Adaptive Galerkin methods with error control for a dynamical Ginzburg-Landau model in superconductivity. *SIAM J. Numer. Anal.* **38**, 1961–1985.
- [14] COLLIANDER, J. E. & JERRARD, R. L. (1998) Vortex dynamics for the Ginzburg-Landau-Schrödinger equation. *IMRN Int. Math. Res. Not.* **7**, 333–358.
- [15] DEANG, J., DU, Q. & GUNZBURGER, M. (2001) Stochastic dynamics of Ginzburg-Landau vortices in superconductors. *Phys. Rev. B* **64**, 52506.
- [16] DEANG, J., DU, Q., GUNZBURGER, M. & PETERSON, J. (1997) Vortices in superconductors: Modeling and computer simulations. *Philos. Trans. R. Soc. Lond. Ser. A* **355**, 1957–1968.
- [17] DU, Q. (1994) Finite element methods for the time dependent Ginzburg-Landau model of superconductivity. *Comp. Math. Appl.* **27**, 119–133.
- [18] DU, Q. (2003) Diverse vortex dynamics in superfluids. *Contemp. Math.* **329** 105–117.
- [19] DU, Q., GUNZBURGER, M. & PETERSON, J. (1992) Analysis and approximation of the Ginzburg-Landau model of superconductivity. *SIAM Rev.* **34**, 54–81.
- [20] DU, Q., GUNZBURGER, M. & PETERSON, J. (1995) Computational simulation of type-II superconductivity including pinning phenomena. *Phys. Rev. B* **51**, 16194–16203.
- [21] DU, Q. & ZHU, W. (2004) Stability analysis and applications of the exponential time differencing schemes. *J. Comput. Math.* **22**, 200–209.
- [22] E, W. (1994) Dynamics of vortices in Ginzburg-Landau theories with applications to superconductivity. *Physica D* **77**, 383–404.
- [23] GLOWINSKI, R. & TALLEC, P. L. *Augmented Lagrangian and Operator Splitting Methods in Nonlinear Mechanics*, SIAM, Philadelphia, PA, 1989.
- [24] JERRARD, R. L. & SONER, H. M. (1998) Dynamics of Ginzburg-Landau vortices. *Arch. Rational Mech. Anal.* **142**, 99–125.
- [25] JIAN, H. Y. (2000) The dynamical law of Ginzburg-Landau vortices with a pinning effect. *Appl. Math. Lett.* **13**, 91–94.
- [26] JIAN, H. Y. & SONG, B. H. (2001) Vortex dynamics of Ginzburg-Landau equations in inhomogeneous superconductors. *J. Differential Equations* **170**, 123–141.
- [27] JIAN, H. Y. & WANG, Y. D. (2002) Ginzburg-Landau vortices in inhomogeneous superconductors. *J. Partial Differential Equations* **15**, 45–60.

- [28] KARAKASHIAN, O. & MAKRIDAKIS, C. (1998) A space-time finite element method for the nonlinear Schrödinger equation: The discontinuous Galerkin method. *Math. Comp.*, **67**, 479–499.
- [29] KWONG, M. (1995) On the one-dimensional Ginzburg-Landau BVPs. *Differential Int. Equations* **8**, 1395–1405.
- [30] LAI, M.-C. & WANG, W.-C. (2002) Fast direct solvers for Poisson equation on 2D polar and spherical geometries. *Numer. Methods Partial Differential Equation* **18**, 56–58.
- [31] LANGE, O. & SCHROERS, B. J. (2002) Unstable manifolds and Schrödinger dynamics of Ginzburg-Landau vortices. *Nonlinearity* **15**, 1471–1488.
- [32] LIN, F.-H. (1996) Some dynamical properties of Ginzburg-Landau vortices. *Comm. Pure Appl. Math.* **XLIX**, 323–359.
- [33] LIN, F.-H. (1998) Complex Ginzburg-Landau equations and dynamics of vortices, filaments, and codimension-2 submanifolds. *Comm. Pure Appl. Math.* **LI**, 0385–0441.
- [34] LIN, F.-H. & DU, Q. (1997) Ginzburg-Landau vortices: Dynamics, pinning, and hysteresis. *SIAM J. Math. Anal.* **28**, 1265–1293.
- [35] LIN, F.-H. & XIN, J. X. (1999) On the dynamical law of the Ginzburg-Landau vortices on the plane. *Comm. Pure Appl. Math.* **LII**, 1189–1212.
- [36] NEU, J. C. (1990a) Vortices in complex scalar fields. *Physica D* **43**, 385–406.
- [37] NEU, J. C. (1990b) Vortex dynamics of the nonlinear wave equation. *Physica D* **43**, 407–420.
- [38] OVCHINNIKOV, Y. N. & SIGAL, I. M. (1997) The Ginzburg-Landau equation I. Static vortices. *Partial Differential Equations Appl. CRM Pro.* **12**, 199–220.
- [39] OVCHINNIKOV, Y. N. & SIGAL, I. M. (1998a) Long-time behaviour of Ginzburg-Landau vortices. *Nonlinearity* **11**, 1295–1309.
- [40] OVCHINNIKOV, Y. N. & SIGAL, I. M. (1998b) The Ginzburg-Landau equation III. Vortex dynamics. *Nonlinearity* **11**, 1277–1294.
- [41] OVCHINNIKOV, Y. N. & SIGAL, I. M. (2000) Asymptotic behaviour of solutions of Ginzburg-Landau and related equations. *Rev. Math. Phys.* **12**, 287–299.
- [42] OVCHINNIKOV, Y. N. & SIGAL, I. M. (2004) Symmetric breaking solutions to the Ginzburg-Landau equation. *J. Exp. Theor. Phys.* **99**, 1090–1107.
- [43] PERES, L. & RUBINSTEIN, J. (1993) Vortex dynamics for U(1)-Ginzburg-Landau models. *Physica D* **64**, 299–309.
- [44] PISMEN, L. & RODRIGUEZ, J. D. (1990) Mobilities of singularities in dissipative Ginzburg-Landau equations. *Phys. Rev. A* **42**, 2471–2474.
- [45] STRANG, G. (1968) On the construction and comparison of difference schemes. *SIAM J. Numer. Anal.* **5**, 505–517.
- [46] TAHA, T. R. & ABLOWITZ, M. J. (1984) Analytical and numerical aspects of certain nonlinear evolution equations II: Numerical, nonlinear Schrödinger equation. *J. Comput. Phys.* **55**, 203–230.
- [47] WEIDEMAN, J. & HERBST, B. (1986) Split-step methods for the solution of the nonlinear Schrödinger equation. *SIAM J. Numer. Anal.* **23**, 485–507.
- [48] WEINSTEIN, M. I. & XIN, J. (1996) Dynamics stability of vortex solutions of Ginzburg-Landau and nonlinear Schrödinger equations, *Comm. Math. Phys.* **180**, 389–428.
- [49] ZHANG, Y., BAO, W. & DU, Q. (to appear) The dynamics and interaction of quantized vortices in Ginzburg-Landau-Schrödinger equation. *SIAM J. Appl. Math.*